Transactions on Engineering and Computing Sciences - Vol. 12, No. 5
Publication Date: October 25, 2024
DOI:10.14738/tecs.125.17572.
Neelakanta, P., & De Groff, D. (2024). Radar Detection of Loitering Drones Via Artificial Neural Networks: A Generative AI Software Support. Transactions on Engineering and Computing Sciences, 12(5). 01-16.

SERVICES FOR SCIENCE AND EDUCATION

Radar Detection of Loitering Drones *Via* Artificial Neural Networks: A Generative AI Software Support

Perambur Neelakanta
Department of Electrical Engineering and Computer Science,
Florida Atlantic University, Boca Raton, Fl. 33431

Dolores De Groff
Department of Electrical Engineering and Computer Science,
Florida Atlantic University, Boca Raton, Fl. 33431

ABSTRACT

The focused effort of this study refers to developing an ANN-based generative AI software towards radar detection of loitering drones in a combat area. Relevant heuristics can provide an adjunct support to a surveillance radar system that remains vulnerable to threats on attacks by low-observable loitering drones. Detection of such drones is necessary for proactive counter actions. In general, a loitering drone implies a suicide munition deployed as an exploding device mimicking kamikaze-style operation at war zones. It is intended to crash on to a vulnerable target such as, a surveillance radar. The present study envisages specifying a compatible radar-specific algorithm towards robust, true-positive detection of menacing drones in a combat zone and adopt an ANN thereof to get trained and predict the estimation of drone-location with an acceptable probability of detection. That is, a test ANN is trained with a set of acquisitioned data pertinent to backscattered signal (echo) received from the drone illuminated by the radar. Compatible ANN of perceptron architecture with backpropagation is indicated and details on compiling necessary data *vis-à-vis* radar detection algorithm towards training and prediction phases (of the ANN) are outlined. Simulation experiments are explained and results are presented to illustrate the efficacy of the test ANN as a generative AI software.

Keywords: Low-observable Target, Radar Cross-section (RCS), Loitering Drones, Detection Probability, Artificial Neural Network, Generative AI**.**

INTRODUCTION

Drones are low-observable, loitering vehicles typically airborne, facilitated with a built-in munition (warhead); and, they are rendered to loiter (move randomly as well as, wait passively) around a specific, vulnerable target (such as a surveillance radar). During loitering, the drone can crash into the radar disenabling its surveillance operation. Drones deployed thereof possess fast reaction times and emerge only for a short-duration posing no obvious exposures to high-value radar platforms deployed in the vicinity of vulnerable surveillance radar. Further, they are designed to loiter in the air for extended periods and conduct autonomous missions. And, they can also seek more selective vulnerable targets (inasmuch as, their mission can be dynamically altered during mid-flight schedules or even aborted). In all,

drones denote a new generation of unmanned aerial vehicles designed to provide "unprecedented levels of flexibility and precision" in killing vulnerable targets, like radars [1]-[6].

The present study is conceived to develop a software support for the surveillance radar in augmenting its capability to detect the drones (for counter measures). The method indicated thereof is to deploy an artificial neural network (ANN) devised in generative AI context. The underlying AI refers to suggesting a class of algorithms that can generate details on loitering drones based on learnt patterns in existing data. Such algorithms are based on adopting ANNs with compatible machine learning algorithm. **Further,** relevant ANN strategy implies fast-convergence capability towards real-time adoptions in pertinent radar detection suites of generative AI. The underlying support of ANN can assist the surveillance radar in detecting low-observable loitering targets possibly equipped with a range of advanced sensors, guidance systems, along with explosive warheads. In view of grossly prone vulnerability of attack by widespread deployment of such menacing drones commissioned in modern hostile and/or warfare ambient, the imminence of this explorative effort towards radar detection *vis-a-vis* small-sized drones, is obvious [7].

METHOD OF APPROACH

The analytical aspect of this study is two-folded: (1) The first task refers to modeling the ambient of a monostatic radar performing surveillance to locate the drone(s) of interest; and, identify a compatible radar detection algorithm to specify the estimation of received (echo) signal power S (watts), backscattered by the drone when illuminated by the radar. Relevantly, the associated radar equation and signal-to-noise ratio (SNR) considerations leading to a robust, true-positive detection of the drone with an acceptable probability of detection, (p_d) in any sector of surveillance interest are addressed. Next, (2) the second exercise includes designing an ANN technique to frame a generative AI compatible software support to serve as an aid to the radar towards robust detection of drones under surveillance**.**

Ambient of Combat-zone with the Presence of Radar and Drone(s)

Consider a geographical area as illustrated in Fig.1. It represents a region of interest subdivided into a suitable number of arbitrary sectors (say, k = 1, 2, …, 6) as shown consistent with prior knowledge on the statistical pattern of loitering of the drone under radar surveillance. Hence as a hypothetical case, the loitering zone is segmented into six sections: k = I through k = IV as shown.

Across this domain of six sectors, the drone(s) to be detected are presumed to loiter randomly. That is, a drone commissioned to attack a vulnerable system (such as a monostatic surveillance radar) can be identified at any instant of time (t) in terms of a spatiotemporal random variable (RV) given by: $L(x, y, z; t)_k$, where (x, y, z) denotes three dimensional (3D) coordinate of the vehicle in the k^{th} sector specified with respect to the origin (0,0,0) (where, the detecting radar is located).

Hence, considering the area (**Ω**) wherein the loitering drones engage in frequent visitations, it is divided into six sectors under surveillance by a monostatic radar located at (0,0) as shown in

Fig.1. Further, each sector is identified with a centroid, **C**; that is, the prime location of loitering cluster pertinent to each of these six sectors of interest is designated as the "centroid". Thus, a set of six (hypothetical) centroids namely, $\{C_I(X_1, Y_1)_{k=1}, C_{II}(X_2, Y_2)_{k=2}, C_{III}(X_3, Y_3)_{k=3}, C_{IV}(X_4, Y_4)_{k=4}, C_V(X_5, Y_5)_{k=5}, C_{IV}(X_6, Y_6)_{k=6}\}$, (where, each coordinate set (X, Y) denotes normalized values (X = x/R, Y = y/R) done with respect to the radial distance, R =10 km) is specified for the segmented six sections. For computational example indicated later, a hypothetical set of centroids thereof is assumed, for example as follows: $\{C_I(X_I, Y_I) = (0.25, 0.25), C_{II}(X_2, Y_2) = (0.40, 0.75), C_{III}(X_3, Y_3) = (-0.20, 0.50), C_{IV}(X_4, Y_4) = (-0.40, -0.20), C_V(X_5, Y_5) = (-0.35, -0.45), C_{VI}(X_6, Y_6) = (0.30, -0.35)\}$.

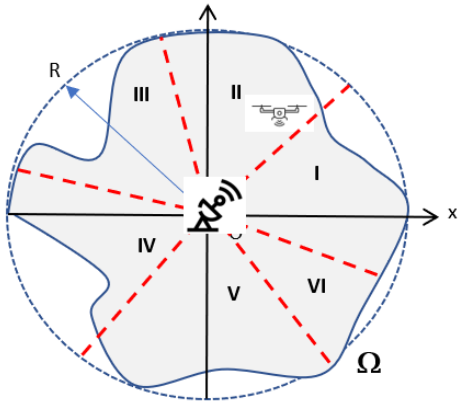


Fig 1: Geographical zone of loitering of a drone with respect to the intercepting monostatic radar: The shaded area (in the domain, Ω) represents statistically observed region of loitering situated within a circle of radius, R meter. The radar facilitated to intercept the drone is located at the origin (0, 0) and it can perform 360° azimuthal surveillance and a vertical scan of 0 to θ_o degrees. The loitering zone is segmented arbitrarily into six sections: k = I through IV as shown.

In all, assuming, the presence of a loitering drone at any instant of time, t is presumably clustered at the centroidal location for any given sector; hence, the location coordinates of the radar at the origin (0, 0, 0) and that of a drone at, L (x, y, z) are illustrated in Fig. 2.

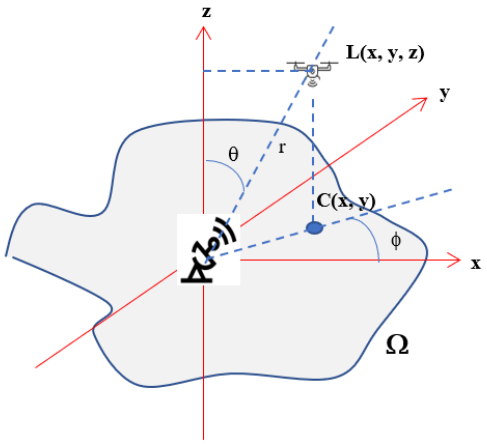


Fig 2: Three-dimensional (3D) view of drone location, L (x, y, z) in any sector of interest with reference to a monostatic radar situated at the origin, (0, 0).

Further, the drone location L (x, y, z) can be equivalently specified also in spherical coordinates L (r, θ, ϕ) where r (m) is the radial distance of the drone from the origin, ϕ is the azimuthal angle and θ is the vertical angle as shown in Fig.2. As mentioned earlier, the loitering drones frequently engage in random visitations clustered around the centroid (of any sector). At any instant of time, t, the loitering drone is identified with reference to the centroidal position **C (**x, y; t) in the azimuthal (x, y) plane of the sector and at a vertical height, z from the xy-plane as shown. Inasmuch as, L(.) is a random variable (RV), it can be specified in terms of its statistical parameters, such as, the probability density function (pdf), p(L), expected average, **E**[L] and corresponding variance, V(L). Since each of these parameters implicitly depends on the spatial coordinate (x, y, z) and time variable, t, $\mathbf{E}[L] = (E_{xyz}[L]) \times (< L >_t)$ where $< (.) >_t$ denotes the time-average. In essence, each sector of interest shown in Fig.1 specified with a centroidal coordinate, C_{ck} $(x_{ck}, y_{ck}, z_{ck})_{k = I \text{ to } VI}$ and each centroid can be attributed with statistical as well as, deterministic parameters relevant to radar detection. That is, each centroidal locations is characterized by a set of following radar-specific parameters: $\{\mathbf{E}[S_k], p_d(S_k), SNR_k, \theta_k, \phi_k\}_{k = I \text{ to } VI}$, where S_k denotes the signal power received at the radar *via* scattered electromagnetic (EM) echo from the drone; and , $p_d(S_k)$ refers to the probability of detection of the target at the intercepting radar, which can be implicitly denoted by the fluctuating radar cross-section (RCS) of the drone [8-12]. The associated signal-to-noise ratio in the detection exercise is denoted by: SNR_k; and, (θ_k, ϕ_k) represent the vertical and horizontal angles of target illumination respectively with reference to a monostatic radar viewing the drone subjected to surveillance.

RADAR DETECTION CONSIDERATIONS

A radar detecting a target is characterized by the well-known radar equation [13-15] as indicated below with reference to a monostatic system where, the target is illuminated by a radar transmitter and the scattered echo signal is received by a unit co-located at the transmitter.

Pertinent to a target (such as a drone) subjected to surveillance by a monostatic radar, the maximum range of the target R_{max} (in meters) is specified by the radar equation given by [13-15]:

$$\mathbf{(R_{max})^4 = \left[\frac{P_T G^2 \lambda^2 \sigma}{(4\pi)^3 S_{min}}\right]} \quad \mathbf{(1)}$$

where,

- P_T; Peak transmitted RF power in watts
- G: Gain of the trans-receive monostatic radar antenna
- λ: Wavelength of RF energy emitted by the radar in meters
- σ: Radar cross-section (RCS) of the target (drone) in meter^2
- S_{min}: Minimum detectable signal power in watts

As well known, the RCS represents a single parameter depicting the stochastic aspects of radar echo signature of the targeted drone. It varies with observation angles, (θ_k, ϕ_k) and may change with the wavelength (λ in meters) of the EM wave used in the radar. Relevant to the present

study focused on drones, some exclusive details on measured/estimated values of RCS (of drones) are available in: [8] and [9].

In lieu of radar-specific parameters: $\{\mathbf{E}[S_k], p_d(S_k), SNR_k, \theta_k, \phi_k\}_{k = I \text{ to } VI}$, designated earlier for six centroids of the sectors (Fig.1) as functions of time (t), an alternative set representing relevant details equivalently, can be specified as,$\{x_k, y_k, z_k, RCS_k, p_d(S_k)\}_{k = I \text{ to } VI}$ with the RCS of the drone viewed at the aspect angles (α_k, β_k) of the drone as seen by the radar at the coordinate angles, (θ_k, ϕ_k) respectively. In general, RCS is a stochastic parameter that has been studied in the past as regard to conventional targets such as, aircrafts and missiles and relevant statistical aspects of RCS parameters have been deeply studied in [16-26]. Specific to low-observable targets, pertinent considerations are indicated by the authors in [11].

Further, given the SNR_k ambient at the radar in detecting the drone, the associated probability of detection, p_d (S_k) can be adopted *in lieu* of prevailing signal-to-noise implications [11], [22], [27]. Thus, the data set $\{X_k, Y_k, Z_k, RCS_k, p_d(S_k)\}_{ki = I \text{ to } VI;\ t}$, cohesively conforms to labeled details corresponding to the six designated centroids; and, the set (X_k, Y_k, Z_k) denotes normalized values ($X_k = x_k/R$, $Y_k = y_k/R$, $Z_k = z_k/R$), where, as stated before, the normalization is done with respect to the maximum radial distance, R = 10 km of the loitering zone of interest).

In terms of drone-specific locational details as outlined above, necessary analytical pursuits on the scope of this study in generative AI perspectives and ANN-based computations can be done as described below:

- Step 1: As indicated above, the initial step refers to identifying a compatible radar detection algorithm to specify the estimation of received echo signal power S_k watts and the associated SNR_k leading to an eventual robust, true-positive detection of the drone with an acceptable probability of detection, $(p_d)_k$ in any k^{th} sector of interest. Correspondingly, an input data set on: $\{x_k, y_k, y_k, RCS_k, (p_d)_k\}_{k = I \text{ to } VI}$ is compiled. Relevant details gathered can further be adopted to generate a set of pseudo-replicates.
- Step 2: To determine the detection status of the loitering drone at a given location, L (x_k, y_k, z_k; t) in any sector, k, it is proposed here to adopt an artificial neural network (ANN), which is first trained with the pseudo-replicates of input details of $\{x_k, y_k, RCS_k, (p_d)_k\}$.
- Step 3: Using the trained test ANN, the task of classifying/verifying whether the ANN output obtained with a fresh input data be considered as highly probable true-positive inference/decision on the presence or absence of the drone at, L (x_k, y_k, z_k; t) in the k^{th} sector under radar surveillance.

Outlined below are details on ANN adopted for the objective exercises as above.

PROPOSED ANN ARCHITECTURE

A possible ANN architecture for use in the proposed scheme is illustrated in Fig.3, where a perceptron with backpropagation and a teacher value (T_i) specified for supervised learning [28-31]; and, specifically, achieving faster convergence in ANNs (as outlined by the authors in [31]), in real-time applications of ANN is emphasized in the present context.

The net of test ANN in Fig. 3 consists of five input units, five neuron units in the hidden layer. The summed/weighted output from the hidden layer is squashed by a nonlinear sigmoidal function, $f(u_i)$; and, the squashed output is linearly scaled (if required with proportional factor K) and presented to a single output unit where the output value O_i is compared against a prescribed teacher value, T_i.

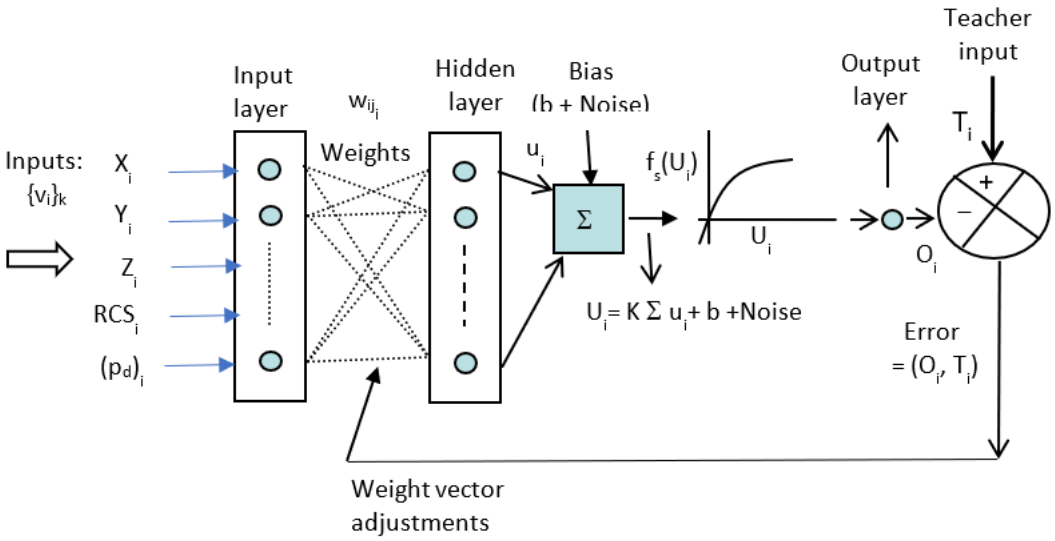


Fig 3: Proposed ANN: Feedforward perceptron with backpropagation and supervised learning

The phases of operation of the test ANN are as follows: The net of Fig. 3 is first trained with the given five input data sets of $\{X_i, Y_i, Z_i, RCS_i, (p_d)_i\}_k$ using the compiled pseudo-replicates of pertinent details on the target (drone) affirmatively loitering within the sectors of interest with $R \leq 10$ km. Subsequent to training the net to convergence, a fresh (arbitrary) input data set is addressed on the net; and,the underlying exercise is to confirm/predict whether, this fresh input data be classified of its belongingness close to the details adopted in training; or, it is an outlier of those details. Relevant classification can be made by observing the learning curve of the fresh input data used. If the data addressed belongs to the details on loitering drone present within the range, $R \leq 10$ km, the resulting learning curve will exhibit convergence towards a global minimum (in concurrence with the known details used in training phase); otherwise, the learning curve will be non-converging implying that the fresh data of the prediction phase belongs to an outlier range $R > 10$ km. Pertinent details thus can provide a software support to the surveillance radar on the presence or absence of the target (drone) within range of interest enclaving the loitering sectors.

Compiling Data for ANN Computations

The data set required for use to train the test ANN can be framed with available details in literature on possible menacing drones. For example, in [8] a comprehensive set of details on measured quasi-monostatic RCS signatures (at 26-40 GHz) of nine different unmanned aerial vehicles (UAV) with multi-rotor platforms each mounted with a lithium-ion polymer battery is presented. Further, in [9] presented are results on RCS measurements of several drones of

nano- and micro-UAV category. In the following table (Table 1), a summary of pertinent data is furnished:

Table 1: Excerpted details from [8][9] on (approximate), average characteristics of certain test drones and their measured RCS signatures

<table>
<tr><td colspan="6">Types of drones: Size, material and features</td></tr>
<tr><td colspan="3">Type I (Small drones)</td><td>VV Min-max RCS m^2</td><td>HH Min-max RCS m^2</td><td>Frequency</td></tr>
<tr><td>Diagonal dimension</td><td>Material</td><td>Feature</td><td rowspan="2">0.01 – 10.00</td><td rowspan="2">0.02 -4.0</td><td rowspan="4">25-50 GHz

Approximate change/increase in RCS
1 m^2 per GHz</td></tr>
<tr><td>300-500 mm</td><td>Plastic</td><td>With Li-ion battery</td></tr>
<tr><td colspan="5"></td></tr>
<tr><td colspan="3">Type II (Large-sized drones)</td><td>VV Min-max RCS m^2</td><td>HH Min-max RCS m^2</td></tr>
<tr><td>Diagonal dimension</td><td>Material</td><td>Feature</td><td rowspan="2">0.10 – 30.00</td><td rowspan="2">0.10 – 10.00</td></tr>
<tr><td>600-900 mm</td><td>Carbon fiber</td><td>With Li-ion battery</td></tr>
<tr><td colspan="6">Note:
VV: (Vertical-Vertical) – Both incident and scattered EM field on the target are in vertical polarizations and the RCS is determined thereof.
HH: (Horizontal-Horizontal) – Both incident and scattered EM field on the target are in horizontal polarizations and the RCS is determined thereof</td></tr>
</table>

Data Compilation

Consistent with the data required at the input layer of the test ANN illustrated in Fig.3, (adopted for drone detection by the radar as described earlier), the required set of data, namely $\{X_i, Y_i, Z_i, RCS_i, p_d(S_i)\}_{k = I \text{ to } VI}$ is compiled by availing relevant details from the literature [8] [9]) and, corresponding pseudo-replicates prepared *via* bootstrapping ("bagging") [32][33].

The compiled data as above refers to six sectors of loitering zones (Fig.1); further, the data on (x_i, y_i, z_i) at each centroid of the sectors is replicated randomly with uniformly distributed values depicting dispersed locales in the vicinity of each centroids. Also, using RCS_i values listed in Table 1, (pertinent to RCS values [8] [9] for small and large-sized drones) necessary details on the input variable, namely $\{RCS_i\}_{k = I \text{ to } VI}$ are designated for the target (drone) loitering proximal to each centroid; further, relevant pseudo-replicates of RCS values are obtained *via* bootstrapping ("bagging"). That is, using the set of available information on RCS, additional pseudo-replicates of RCS values are determined *via* statistical bootstrap aggregation as described in [32] [33].

Next, considering the probability of detection, $\{(p_d)_i\}_{k = I \text{ to } VI}$, it is randomly assigned to each drone location under radar surveillance within the minimum-to-maximum bounds of 0.85 to 0.95, ensuring a robust prediction towards true-positive detection. The statistics pursued thereof conforms to unbiased uniform distribution of $(p_d)_i$ values prescribed.

Further, consistent with the min-max values of $(p_{dj})_i$ presumed as (0.85 - 0.95), the associated median value of 0.90 is taken as the teacher value, T_i shown in Fig. 3. It refers to an acceptable median value on the probability of detection $(p_d)_i$ towards which the ANN should converge in its training schedule.

Hence, Table 2(a) is constructed with a compilation of data on the set $\{X_i, Y_i, Z_i\}_{k = I \text{ to } VI}$ for Type I (small-sized) or Type II (large-sized) drone detection at locations in the six sectors shown in Fig.1.

Table 2(a): Normalized set of centroidal coordinates of the drone $\{x_i, y_i, z_i\}_{k = I \text{ to } VI}$ and their clustered dispersions (in the vicinity of the centroids)

Normalization: $(x_i/R)_{k = I \text{ to } VI} = (X_i)_k$, R = 10 km						
	Sector I	Sector II	Sector III	Sector IV	Sector V	Sector VI
	X_1	X_2	X_3	X_4	X_5	X_6
Randomly dispersed values in the vicinity of centroids	0.28	0.40	–0.28	–0.40	–0.35	0.30
	0.25	0.38	–0.22	–0.43	–0.37	0.29
	0.27	0.36	–0.24	–0.44	–0.38	0.31
	0.29	0.42	–0.23	–0.43	–0.36	0.28
	0.29	0.42	–0.23	–0.43	–0.36	0.28
Normalization: $(y_i/R)_{k = I \text{ to } VI} = (Y_i)_k$, R = 10 km						
	Y_1	Y_2	Y_3	Y_4	Y_5	Y_6
Randomly dispersed values in the vicinity of centroids	0.29	0.75	0.39	–0.20	–0.45	–0.35
	0.28	0.78	0.38	–0.25	–0.40	–0.37
	0.22	0.69	0.36	–0.22	–0.41	–0.36
	0.24	0.72	0.36	–0.26	–0.44	–0.38
	0.27	0.74	0.35	–0.21	–0.43	–0.39
Normalization: $(z_i/R)_{k = I \text{ to } VI} = (Z_i)_k$, R = 10 km						
$z_i/R = Z_i$	Z_1	Z_2	Z_3	Z_4	Z_5	Z_6
Randomly dispersed values in the vicinity of centroids	0.66	0.50	0.79	0.60	0.75	0.99
	0.60	0.55	0.80	0.60	0.70	1.00
	0.65	0.54	0.85	0.63	0.71	0.98
	0.68	0.50	0.77	0.65	0.74	0.89
	0.69	0.56	0.75	0.61	0.75	1.00
Remarks: As indicated, the normalization parameter used on (x, y, z) refers to the range, R = 10 km that includes all loitering sectors Altitudes (z) of loitering drones in the combat area: 15,000 feet (~ 5 km) to 25,000 feet (~8 km) where the drones can stay aloft for more than forty hours [34].						

Further, furnished below are Tables 2(b) and 2(c), which include compiled and pseudo-replicated details on RCS values$\{(\sigma_B)_i\}_{k = I \text{ to } VI}$ (in m^2) that are presumed to be possibly estimated at the border/edge of the loitering zone (at R = 10 km). Tables 2(b) contains pseudo-replicates

of RCS values $\{(\sigma_B)_i\}_{k = I \text{ to } VI}$ of small drones; and, Tables 2(b) refers to such values on large-sized drones.

Table 2(b): RCS values (in m^2), $\{(\sigma_B)_i\}_{k = I \text{ to } VI}$ of small-drones presumed to exist at the border/edge of the loitering zone (at R = 10 km) and their pseudo-replicates

RCS data for Type 1 (small-sized) drones [8][9]						
	Sector I	Sector II	Sector III	Sector IV	Sector V	Sector VI
RCS values $\{(\sigma_B)_i\}_{k = I \text{ to } VI}$ (in m^2) and pseudo-replicates	RCS_1	RCS_2	RCS_3	RCS_4	RCS_5	RCS_6
	0.050	0.250	0.200	0.600	0.730	0.660
	0.730	0.660	0.001	0.200	0.050	0.250
	0.660	0.001	0.200	0.800	0.001	0.200
	0.200	0.800	0.400	0.600	0.660	0.001
	0.600	0.660	0.200	0.001	0.200	0.200

Table 2(c): RCS values (in m_2), $\{(\sigma_B)_i\}_{k = I \text{ to } VI}$ of large-drones presumed to exist at the border/edge of the loitering zone (at R = 10 km) and their pseudo-replicates

RCS data for Type 2 (large-sized) drones [8][9]						
	Sector I	Sector II	Sector III	Sector IV	Sector V	Sector VI
RCS values $\{(\sigma_B)_i\}_{k = I \text{ to } VI}$ (in m^2) and pseudo-replicates	RCS_1	RCS_2	RCS_3	RCS_4	RCS_5	RCS_6
	0.453	0.667	0.333	0.600	0.733	1.000
	0.733	1.000	0.453	0.667	0.600	0.733
	0.167	0.333	0.167	0.333	0.333	0.167
	0.333	0.333	0.167	0.167	0.333	0.167
	0.667	0.600	0.733	1.000	0.453	0.667

Table 2(d): Presumed $\{(p_d)_i\}_k$ values designated as $(p_{dE})_k$ at the edge of the loitering zone (that is, at the maximum range, R = 10 km) and their pseudo-replicates in the case of small-sized drone detection

	$(p_{dE})_1$	$(p_{dE})_2$	$(p_{dE})_3$	$(p_{dE})_4$	$(p_{dE})_5$	$(p_{dE})_6$
	0.25	0.25	0.30	0.29	0.35	0.30
(Min – Max 0.20 – 0.40)	0.35	0.30	0.29	0.35	0.25	0.25
	0.29	0.35	0.30	0.25	0.25	0.30
	0.35	0.30	0.25	0.25	0.30	0.29
pseudo-replicates	0.30	0.29	0.35	0.25	0.30	0.29

Min-Max values (0.20 – 0.40) of probability of detection (p_{dE}) are taken for possible detection objective considerations at the edge of the loitering zone (at R = 10 km)
Assigned pseudo-replicates of $(p_{dE})_k$ thereof, correspond to a set of uniformly distributed values in the Min-Max range: (0.20 – 0.40)
Corresponding teacher value (T_i) is taken as p_d-value at the location of the drone, $0 < r < R$) for robust detection. Say, $T_i = 0.90$.

Table 2(e): Presumed $\{(p_d)_i\}_k$ values designated as $(p_{dE})_k$ at the edge of the loitering zone (that is, at R = 10 km) and their pseudo-replicates in the case of large-sized drone detection

	$(p_{dE})_1$	$(p_{dE})_2$	$(p_{dE})_3$	$(p_{dE})_4$	$(p_{dE})_5$	$(p_{dE})_6$
(Min – Max	0.35	0.40	0.35	0.39	0.38	0.35

0.30 – 0.50)	0.39	0.38	0.35	0.35	0.40	0.35
	0.29	0.35	0.39	0.38	0.25	0.30
pseudo-replicates	0.35	0.30	0.25	0.25	0.30	0.29
	0.25	0.25	0.30	0.30	0.25	0.25
Min-Max values (0.30 – 0.50) of probability of detection (p_{dE}) are taken for possible detection objective considerations at the edge of the loitering zone Assigned pseudo-replicates of $(p_{dE})_k$ thereof, correspond to a set of uniformly distributed values in the Min-Max range: (0.30 – 0.50) Corresponding teacher value (T_i) is taken as p_d-value at the location of the drone, (0 < r < R) for robust detection. Say, T_i = 0.90.						

Further, at any location of the drone in the range, (0 < r < R), the value of p_d adopted for use in test ANN namely, $[\{(p_d)_i\}_k]_{0<r<R}$, is normalized with the following heuristics on normalization: Inasmuch as the detection probability degenerates inversely with respect to target range, $[\{(p_d)_i\}_k]_{0<r<R} = (R/r) \times (p_{dE})_i$.

ANN Simulation

The underlying simulation of the test ANN: Feedforward perceptron with backpropagation (of Fig.3), the following pseudocode is presented to illustrate the computational steps. Subsequently, results obtained with a set of sample inputs are indicated and discussed.

Pseudocode

Compile

Input data set

Identify: Sector number: (k = 1, 2, …, 6)

Specify: Input variable for the Sector k

R = 10 km, x_i km$_i$, y_i km, z_i km, $(\sigma_B)_i$ m^{2}and $(p_{dE})_I$ – from Tables 2(a) and 2(b)

Compute: For a given Sector k,

$$r\ (km) = [(x_i)^2 + (y_i)^2]^{1/2}$$

Evaluate: Normalized values of:

$x_i/R = X_i$, $y_i/R = Y_i$, $z_i/R = Z$, $(\sigma_i)_r = \{(\sigma_B)_i\} \times (r/R)^{1/4}$, and $(p_{di})_r = (R/r) \times (p_{dE})$

Import

Input data set for any Sector k: Tables 2(a) and 2(b)

Compile

Set of normalized values for use as inputs at the test ANN (Fig. 3): $\{v_i\}_k$

Define [5 × 1] Input matrix: $[\mathbf{v_i}]_\mathbf{k} = \begin{bmatrix} \mathbf{X_i} \\ \mathbf{Y_i} \\ \mathbf{Z_i} \\ (\boldsymbol{\sigma_i})_\mathbf{r} \\ (\mathbf{p_{di}})_\mathbf{r} \end{bmatrix}$

Training Phase

Step I: Initialization – Ref: Fig. 3

Identify [5 × 5] = 25 interconnecting weights between input and hidden layers

Weight set: $\{w_{ij}\} = w_{11}, w_{12}, w_{13}, \ldots, w_{53}, w_{54}, w_{55}\}$

$$\text{Weight Matrix } [\mathbf{w_{ij}}] = \begin{bmatrix} \mathbf{w_{11}} & \cdots & \mathbf{w_{15}} \\ \vdots & & \vdots \\ \mathbf{w_{51}} & \cdots & \mathbf{w_{55}} \end{bmatrix}$$

Prescribe

Initial weight coefficients

Assign uniformly-distributed random value in the limit: (–1 to +1) for each interconnection weight

Compute

(Input matrix × Transpose of weight matrix): $\mathbf{u_i} = [\mathbf{v_i}]_\mathbf{k} \times [\mathbf{w_{ij}}]^\mathbf{T}$

Evaluate

Sum values of the product: (Input matrix × Transpose of weight matrix)

$$\sum_{i=1}^{5} \mathbf{u_i} = \sum_{i}^{5} [\mathbf{v_i}]_\mathbf{k} \times [\mathbf{w_{ij}}]^\mathbf{T}$$

Modify

The deduced sum, $\sum_{i=1}^{5} \mathbf{u_i}$ is further modified with the addition of a bias of constant value, "b" and/or a random "noise" so as to get: U_i. (Addition of noise conforms to any analytical need to implement the presence of radar signal perturbations due to operational/clutter-prone EM ambient. The probability distribution of the noise can be chosen to meet the radar signal plus clutter profile in the echo received). Hence,

$$U_i = K \sum_{i=1}^{5} \mathbf{u_i} + b + \text{Noise}$$

Next

Perform sigmoidal squashing on the evaluated U_i.

Standard sigmoidal functions such as $\tanh(\beta U_i)$ with β denoting a gain or smearing parameter or the Langevin-Bernoulli function, $L_Q(U_i)$ with Q depicting an order parameter on the stochastic aspects of the variable, U_i [28] [29].

Evaluate

Statistical distance between the squashed value of U_i namely, O_i and the prescribed teacher value, T_i in the output layer so as to arrive at an error function, $\varepsilon(O_i, T_i)$. The functional format of $\varepsilon(.)$ can be any standard distance/divergence function such as, Manhattan distance, Mahalobonis measure, Kullback-Leibler (KL) distance etc. [29] or simple Euclidean measures like, $|O_i - T_i|$ or root-mean squared value, $(\text{RMSE}) = \sum_n^N [(O_n - T_n)^N]^{1/2}$ etc.

Implement

Backpropagation of the error function applied onto the interconnection weights $\{\mathbf{w_{ij}}\}$ *via* a compatible algorithmic rule such as perceptron learning rule

Hence, update weights using the perceptron learning rule

Compute

Converged weights matrix

By performing backpropagation-based procedure towards updating the weight matrix iteratively for the entire set of input values considered for training phase

Hence, obtain the final converged weights matrix

Plot

Concurrently, plot the learning curve: Error *versus* iterations for the last set of training inputs so as to visualize the associated learning-curve.

Prediction Phase

Input data set

For prediction decisions

- Specify**:** Two sets of input variables

Set (i): This corresponds to input values of $\{X_i, Y_i, Z_i, RCS_i, p_d(S_i)\}_{k = I \text{ to } VI}$ within the maximum range, R = 10 km in the loitering zone

Set (ii): This corresponds to input values of $\{X_i, Y_i, Z_i, RCS_i, p_d(S_i)\}_{k = I \text{ to } VI}$ outside the maximum range, R = 10 km, specified as outlier locations

Prescribe

Interconnection weight coefficients corresponding to the final converged weights matrix determined in the training phase

Compute

Apply fresh input data sets designated as Sets(i) and (ii) as above.

Evaluate

Learning curves: (Error *versus* iterations) for each case of Sets (i) & (ii) so as to visualize the underlying learning-curves.

Plot

Learning curves of training and prediction phases

END

RESULTS, DISCUSSIONS AND CONCLUDING REMARKS

The thematic aspect of this study refers to the scope of developing a generative AI software support for a radar system operated in a combat zone where, hostile drones may loiter and pose critical weapon threats to the radar ambient. Typically, such drones as described earlier, can be loitering anywhere within a maximum radial distance from the radar. As such, it is necessary to assist the radar (during its surveillance mission) in terms of signal parameters assessed at the radar receiver and possibly invoking AI schemes) so as to confirm the presence/absence of loitering targets.

In the present study, a monostatic radar placed in a loitering zone is considered with a maximum surveillance range of R = 10 km. The location (L) of a loitering drone under surveillance, is specified in terms of its xy-coordinates, $(X_i, Y_i)_k$ in six (arbitrary) azimuthal sectors (k = I to VI) and at a vertical height $(Z_i)_k$, as described earlier. In all, the parameters availed from the radar receiver conform to $\{X_i, Y_i, Z_i, RCS_i, p_d(S_i)\}_{k = I \text{ to } VI}$ with $[RCS_i]_k$ depicting the radar cross-section of the drone observed at any location of interest; and, $[p_d(S_i)]_k$ denotes the probability of detection enabled by the echo signal S_i at the radar receiver.

Hence, using relevant data as presented in Tables 2(a)-2(e), the test ANN is trained; and, the converged weight matrix is obtained and stored. Next, using this set of converged weight coefficients, the prediction phase exercise on the test ANN is done to obtain the associated learning curves.

Two prediction sets are considered thereof:

1. The first set refers to drone-location details (at the centroids of the six sectors) within the maximum range of R = 10 km.
2. The second prediction phase learning curves assessed refer to arbitrary outlier locations at R > 10 km in four quadrants surrounding the radar.

The computed results on (i) and (ii) as above are presented in Figs. 5 and 6 respectively. The results indicated in Fig. 5 conforms to prediction phase results of (i) on learning curves based on drone-location details at ranges less than 10 km. Relevant learning curves show consistently converging trends for any sector implying that the data received at the ANN input leads to an output (O_i) matching the teacher value (T_i) with a minimum (acceptable) error prescribed on the desired probability of detection, $[p_d\ (S_i)]_k$.

The prediction phase results of (ii) are shown in Fig. 6 assessed on arbitrary outlier locations of the drone at R > 10 km in four quadrants surrounding the radar. Pertinent suite of computed learning curves indicates non-converging trends for any quadrant location, implying that the data received at the ANN input does not lead to an output (O_i) towards the teacher value (T_i) prescribed on desired probability of detection, $[p_d\ (S_i)]_k$. That is, the drone location is not perceivable for any radar-specific actions.

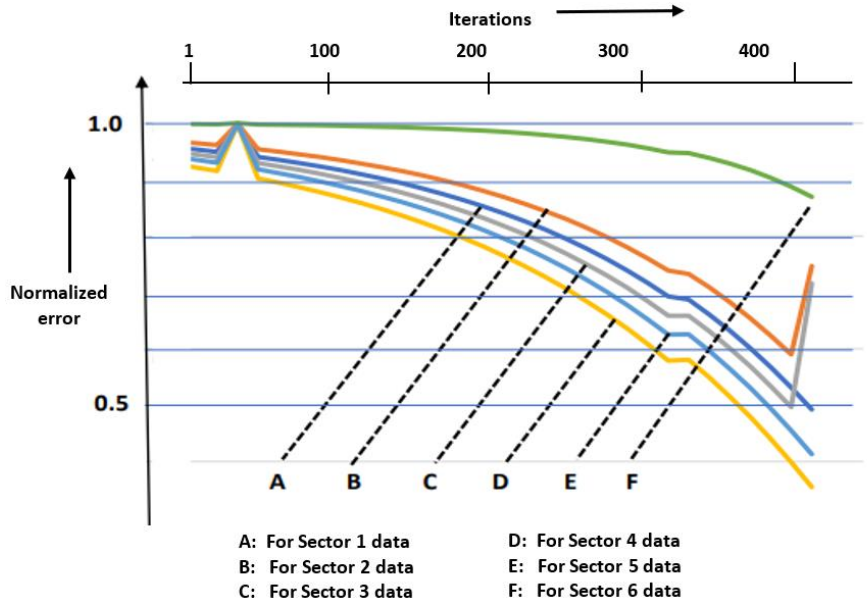


Fig 5: Prediction phase results on learning curves based on drone-location details at ranges less than 10 km in any sectoral region

Thus, given an input set of details on $\{X_i, Y_i, Z_i, RCS_i, p_d(S_i)\}_{k = I \text{ to } VI}$ with $[RCS_i]_k$ applied on the trained ANN, the observed ANN output provides an alert on the presence of a drone in the region with R < 10 km; likewise, for any drone loitering beyond the circumference of radius R > 10 km in any quadrant surrounding the radar, the radar is kept in no-action mode.

In conclusion, the software support outlined in this study offers an ANN-based strategy that can be adopted at the radar receiver to make predictions on the presence or absence of a drone in a loitering zone (so as to pursue any counter actions as needed). The underlying generative AI refers to supervised algorithms adopted towards enabling a computer system to use existing contents on radar parameters and predict possible output details on (unknown) drone-locations, when fresh radar-detection parameters are addressed at the ANN input; hence, the underlying idea refers to AI-implied generation of output artifacts that would resemble the details acquired in the supervised learning phase of the ANN.

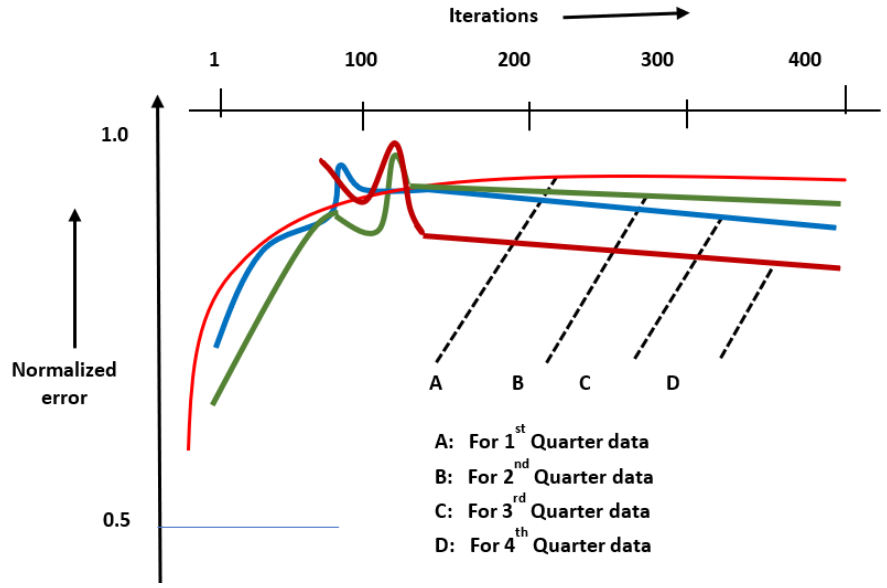


Fig 6: Prediction phase results of on learning curves based on drone-location details at ranges greater than 10 km in any quadrant surrounding the radar

In all, the generative AI with neural network, can capture complex, high-level abstractions from the input data (on radar detection parameters) during supervised learning phase, and generate new, realistic contents in the prediction phases. That is, the neural network plus generative AI can take available insights to simulate and predict fresh information pertinent a virtual drone environment facilitating actual countermeasures as required [35].

References

[1]. D. Gettinger and A.H. Michel: CSD-Loitering Munitions. Report: Center for the Study of the Drones at the Bard College, 2017. Available at: *chromeextension://efaidnbmnnnibpcajpcglclefindmkaj/https://dronecenter.bard.edu/files/2017/02/CSD-Loitering-Munitions.pdf*

[2]. Uvision- Smart Loitering Systems, 2010. Available at: i*nfo@uvisionuav.com*

[3]. Z. Zhang et al.: Research on Speed Scheme for Precise Attack of Miniature Loitering Munition. *Mathematical Problems in Engineering* vol. 2020, Article ID 4963738, 19 pages *https://doi.org/10.1155/2020/4963738*

[4]. S. Lyson: Switchblade Drones: The Role of Miniature Loitering Munitions in Modern Reconnaissance. ExecutiveGov: Digital News Coverage of Government Contracting and Federal Policy Landscape (April 11, 2024). Available at: *https://executivegov.com/articles/switchblade-drones-modern-reconnaissance/*\

[5]. W. K. J. Tang: Systems Analysis of Sense and Strike Capabilities within an Armored Combat Unit in an Offensive Urban Operation. *M.S. (Systems Engineering) Thesis*, Naval Postgraduate School, September 2022, Monterey, CA: USA

[6]. The 911 Security Monthly Newsletter: Radar Drone Detection: Detect Drones Using Radar Sensors. Available at: *https://www.911security.com/en-us/knowledge-hub/drone-detection/radar*

[7]. B. Taha and A. Shoufan: Machine Learning-based Drone Detection and Classification: State-of-the-art in Research. *IEEE Access*, 2019, pp. (99):1-1

[8]. V. Semkin, et al.: Analyzing Radar Cross Section Signatures of Diverse Drone Models at mmWave Frequencies. *IEEE Access* (Special Section on Millimeter-wave and Terahertz Propagation, Channel modeling and Applications, vol.8, 2020, 48958-48969.

[9]. P. Sedivy and O. Nemec: Drone RCS Statistical Behaviour. NATO STO MSG-SET-183 Specialists' Meeting, April 27, 2021, Virtual Web Seminar on Drone Detectability: Modelling the Relevant Signature. Available At: *MP-MSG-SET-183-04%20(1).pdf*.

[10]. H. Lee et al.: DDPG-based Deep Reinforcement Learning for Loitering Munition Mobility Control: Algorithm Design and Visualization. 2022 IEEE VTS Asia Pacific Wireless Communications Symposium (APWCS), 24-26 August 2022., Seoul, Republic of Korea. DOI: 10.1109/APWCS55727.2022.9906493

[11]. P. S. Neelakanta and D. De Groff: Assessment of RCS-specific SNR and Loglikelihood Function in Detecting Low-observable Targets and Drones Illuminated by Low Probability of Intercept Radar Operating in Littoral Regions. *Transactions on Networks and Communications*, 2021, vol.9(4), 1-22.

[12]. S. Chen, P. Huang and J. Ji: Radar Cross Section Fluctuation Characteristics of Typical Stealth Aircraft. *Hangkong Xuebao/Acta Aeronautica et Astronautica Sinica, 2014, 35(12), pp.3304-3314*

[13]. M. I. Skolnik: *Introduction to Radar Systems*. McGraw-Hill, NY: USA, 1982.

[14]. B. R. Mahafza: *Radar Systems Analysis and Design Using MATLAB*. Chapman & Hall/CRC, Boca Raton, FL: USA, 2000

[15]. P. Lacomme, et al.: *Air and Spaceborne Radar Systems: An Introduction*. 2001 William Andrew Publishing LLCX, Norwich, NY: USA

[16]. T. Parthasarathy and P. S. Neelakantaswamy: Statistical Aspects of Radar Cross-section Analysis. *Electro Technology*, Jan./Feb. 1972, pp.21-27.

[17]. J. I. Marcum: A Statistical Theory of Target Detection by Pulsed Radar. *IRE Transactions on Information Theory*, IT-6, 1960, 59—267.

[18]. P. Swerling: Probability of Detection for Fluctuating Targets. Technical Report RM-1217, Rand Corporation, March 17, 1954.

[19]. P. Swerling: Probability of Detection for Fluctuating Targets. *IRE Transactions on Information Theory*, IT-6, 1960, 269—308.

[20]. P. Swerling: More on Detection of Fluctuating Targets. *IRE Transactions on Information Theory*, IT-11, 1965, 459—460.

[21]. P. Swerling: Recent Developments in Target Models for Radar Detection Analysis*. 1970 AGARD Avionics Tech. Symposium Proceedings*, Istanbul, Turkey, May 25—29, 1970.

[22]. D. A. Shnidman: Determination of Required SNR Values Radar Detection. *IEEE Transactions on Aerospace and Electronic Systems, 2002*, vol. 38, no. 3, pp. 1059-1064.

[23]. S.K. Chatterjee, P. S. Neelakantaswamy and Chatterjee, R., Measurement of Back-scattering Cross-sections of Metallic Bodies of Revolution at X-band. *Journal of Institution of Engineers* (India), ET-9, 1969, pp. 87-93.

[24]. P. H. R. Scholefield: Statistical Aspects of Ideal Radar Targets, *Proceedings of the IEEE,* 1967, 55(4), pp. 587-589.

[25]. X. Song, W. Blair and S. Zhou: Dominant-plus-Rayleigh Models for RCS: Swerling III/IV versus Rician, *IEEE Transactions on Aerospace and Electronic Systems*, 2013, 49(3), pp.2058-2064.

[26]. P. S. Neelakanta, D. De Groff and R. Sudhakar: Low-altitude Target Detection by Coastline Operated Marine Radar. *IEEE Trans. Aerospace Electronic System*, 1992, 28(1), pp. 217-222.

[27]. Q. Yang, et al.: Parameter Estimation of the Processing Targets with a Wideband Terahertz Radar, *2018 43rd International Conference on Infrared, Millimeter, and Terahertz Waves (IRMMW-THz)*, Nagoya, Japan, 2018, pp. 1-2, doi: 10.1109/IRMMW-THz.2018.8510474.

[28]. P. S. Neelakanta and D. De Groff: *Neural Network Modeling: Statistical Mechanics and Cybernetic Perspectives*. CRC Press, Inc., Boca Raton, Fl.: 1994

[29]. P. S. Neelakanta: *Information Theoretic Aspects of Neural Networks*, CRC Press, Inc., Boca Raton, Fl.: 1999

[30]. P. S. Neelakanta, M. Dabbas and D. De Groff: Technoeconomic Projections with Artificial

[31]. Neural Networks Using an Ensemble of sparsely-sampled Bootstrapped Data. *British Journal of Economics, Management and Trade*, vol.4(2), 2014, 228-263.

[32]. D. De Groff and P. S. Neelakanta: Faster Convergence Artificial Neural Networks. *International Journal of Computers and Technology*, 2018, vol.17(1), 7126-7132

[33]. Y. Jia and T. Culver: Bootstrapped Artificial Neural Networks for Synthetic Flow Generation with a Small Data Sample, *Journal of Hydrology*; vol 331(34), 2006, pp 580-590.

[34]. B. Efron: Bootstrap Methods: Another Look at the Jackknife, *Annals of Statistics*, vol 7(1), 1979, pp 1-26.

[35]. W. M. Arkin: Loitering with Intent. Harper' Magazine. Available at: *https://harpers.org/archive/2015/06/loitering-with-intent/*

[36]. Dosha Note: Generative AI vs. Neural Networks: Exploring the Landscape. Sept 23, 2023. Available at: *https://dasha.ai/en-us/blog/generative-ai-vs-neural-networks-exploring-the landscape#:~:text=Neural%20Networks%20are,amounts%20of%20data.*